Materials Science inc. Nanomaterials & Polymers

Mussel-Inspired Surface Acrylation on Graphene Oxide Using Acrylic Surface Primers and Its Hydrogel-Based Applications: Sustained Drug Release and Tissue Scaffolds

Kyu Ha Park,[a] Jaewon Jung,[a] Sang-Gu Yim,[a] Mi Ju Kang,[a] Gibum Kwon,[b] Dae Youn Hwang,[a] Seung Yun Yang,[a] and Sungbaek Seo*[a]

Composite hydrogels integrated with graphene oxide were prepared to enable the sustained release of loads for graphene-based aromatic drug delivery and enhanced cell adhesion for tissue scaffolds. The surface of graphene oxide was readily transformed by the adsorption of acrylic surface primer (SP) without chemical reactions. The surface modification was verified by energy dispersive X-ray spectroscopy and X-ray diffraction spectra. The acrylated graphene oxide (SP-GO) was photocrosslinked with acrylate groups of poly(ethylene glycol) to generate a composite hydrogel (SP-GO hydrogel). Based on the molecular weight of poly(ethylene glycol), the hydrogels showed a swelling ratio range of ~5–20, respectively. The SP-GO did not change noticeably mechanical properties and inner structures of the hydrogels. Aromatic doxorubicin (DOX) was entrapped in the hydrogels with good yield and demonstrates the potential for a drug delivery carrier. The released DOX from the hydrogel containing SP-GO (70.56% of entrapped DOX) exhibited a sustained release profile with reduced release after five days in a wet environment compared to the released DOX from a hydrogel without SP-GO (92.29% of entrapped DOX). DOX is supposed to be attracted to graphene oxide and is physically entrapped inside the hydrogels. Moreover, bone MG-63 cells entrapped in the SP-GO hydrogel showed increased TGF-β and fibronectin expression levels. This implies that SP-GO contributes to enhancing cell growth and adhesion by providing cell-laid structural support.

1. Introduction

Graphene-based nanomaterials are attractive owing to their unique physicochemical properties such as high intrinsic mobility, large surface area, high thermal and electrical conductivity, and mechanical strength.[1–3] In particular, graphene oxide (GO) has polar groups containing oxygen (e.g., hydroxyl, carbonyl, and epoxide groups) at the basal plane, providing binding sites on its surface. However, for practical applications, the polar groups of GO should be chemically modified or consistently functionalized. For example, to adsorb CO_2 efficiently, imine-functionalization of GO is required through a silanization reaction with the hydroxyl groups of GO, following the Schiff base condensation reaction.[4] Alkylation of GO is needed to construct a lubricant via a coupling reaction of the alkylamine with the carboxylic groups of GO.[5] These approaches for surface functionalization include reactions requiring toxic chemicals and time-consuming processes. In contrast, simple coating methods using nature-inspired (poly) phenolic molecules is an alternative to the surface modification of many organic and inorganic substrates.[6–10] Phenolics have been used on a variety of substrates through adhesion mechanisms, such as strong bidentate hydrogen bonds or/and coordination bonds, to oxidized substrates[11,12] which together build complex bulk adhesion.[13–15] The mussel-inspired phenolic (or catecholic) polymer binders are used for surface modification of silicon nanoparticles in high-performance lithium-ion batteries.[16] The phenolic zwitterionic surfactants are used on nano-grooved dielectric substrates as surface modifiers to produce organic field-effect transistors.[17] In our previous research, a single-surface primer containing phenolic and acrylic groups enabled adherence to silica fillers that enhanced the toughness of the composite consisting of filler and polymer resin by interfacial bridging to the acrylic resin.[18]

Currently, GOs have been utilized in biomedical applications, such as drug delivery, biosensing, bioimaging, and tissue engineering.[1,3,19–22] In particular, GOs have been developed as nanocarriers for efficient loading and delivery of aromatic drugs, such as doxorubicin (DOX),[1,23,24] with benefits of a high surface area of GO and binding sites consisting of π-π stacking interactions between DOX and GO. The challenge in developing DOX delivery nanocarriers is controlling the loading efficiency, delivery, and release of the aromatic drug. For example, to overcome this limitation, the release of DOX within polyethylene glycol (PEG)-coated GO was triggered by glutathione, weakening the aromatic interactions between the drug and PEGylated GO.[24] Another approach used to control the release of DOX in GO-based nanocarriers is to exploit pH-

[a] K. H. Park, J. Jung, S.-G. Yim, M. J. Kang, Prof. D. Y. Hwang, Prof. S. Y. Yang, Prof. S. Seo
Department of Biomaterials Science, College of Natural Resource and Life Sciences / Life and Industry Convergence Institute, Pusan National University, Miryang 50463, Republic of Korea
E-mail: sbseo81@pusan.ac.kr
[b] Prof. G. Kwon
Department of Mechanical Engineering, University of Kansas, Lawrence, Kansas 66045, United States

Supporting information for this article is available on the WWW under https://doi.org/10.1002/slct.202000205

© 2020 Wiley-VCH Verlag GmbH & Co. KGaA, Weinheim

responsive dissociation of DOX in the cytoplasm (pH 5.0–6.5) of cancer cells.[25]

Hydrogel- or composite hydrogel-based drug carriers are suitable systems for controlled or sustained delivery due to manageable pore size and swelling behavior.[26–29] For instance, L-alanine-based low molecular weight hydrogelators entrapping DOX remained injectable and sustained in vivo delivery of DOX.[30] A self-assembled nanofiber of synthetic peptide and DOX form a hydrogel, enabling the release of DOX in a sustained manner.[31]

GOs have been used with PEG-based hydrogels[32–34] for tissue-engineered scaffolds. GO-embedded hydrogels enhance stem cell growth and adhesion.[35–37] In particular, GOs have been revealed to assist stem cell adhesion, growth, and differentiation by providing binding or adhesion sites. However, these studies require chemical reactions such as covalent conjugation to crosslink to the PEG gel networks. Approaches enabling GO crosslinking to PEG hydrogels without a chemical reaction have rarely been attempted.

Herein, we apply surface priming on GO using an acrylic surface primer that has a catechol adhesive directed towards oxidized substrates to provide a surface primed GO (SP-GO) with the acrylate groups exposed (Figure 1).

The acrylates of SP-GO enable integration with PEG diacrylates via photocrosslinking, yielding a composite hydrogel containing an SP-GO (SP-GO PEG hydrogel). An aromatic DOX was blended with SP-GO/PEG diacrylate mixture in aqueous solution to load aromatic compounds in the hydrogel. Compression tests compared the mechanical properties of the hydrogels with or without SP. The loading efficiency of DOX in the hydrogels and time-dependent release profiles of DOX from the hydrogels were evaluated when low- and high-molecular weight PEG diacrylate was used. Furthermore, the amount of TGF-β and fibronectin expression, which is related to cell adhesion and proliferation, were evaluated between SP-GO PEG hydrogel and PEG hydrogel without GO.

2. Results and Discussion

A reaction-free surface acrylation on GO was prepared using the surface priming method[18] and an acrylic surface primer. The morphologies and elements of GO and SP-GO were examined using TEM images and EDS analysis as shown in Figure 2a.

The morphologies of GO and SP-GO were fragment-like structures with a 2–3 μm size. The C/O atomic ratio (8.58) of the SP-GO was higher than that (5.61) of GO, indicating that the surface of GO was transformed by the adsorption of the acrylic surface primer containing a large number of carbon atoms. Surface morphologies and height profiles of GO and SP-GO were analyzed by AFM (Figure 2b and **Figure S1**). Irregular fragment-like surface structures of GO and SP-GO were observed, and the 100–200 nm height of both samples were comparable. XRD spectra were recorded (Figure 2c) to investigate the structural changes in the surface of GO caused by surface priming and to examine the intermolecular packing

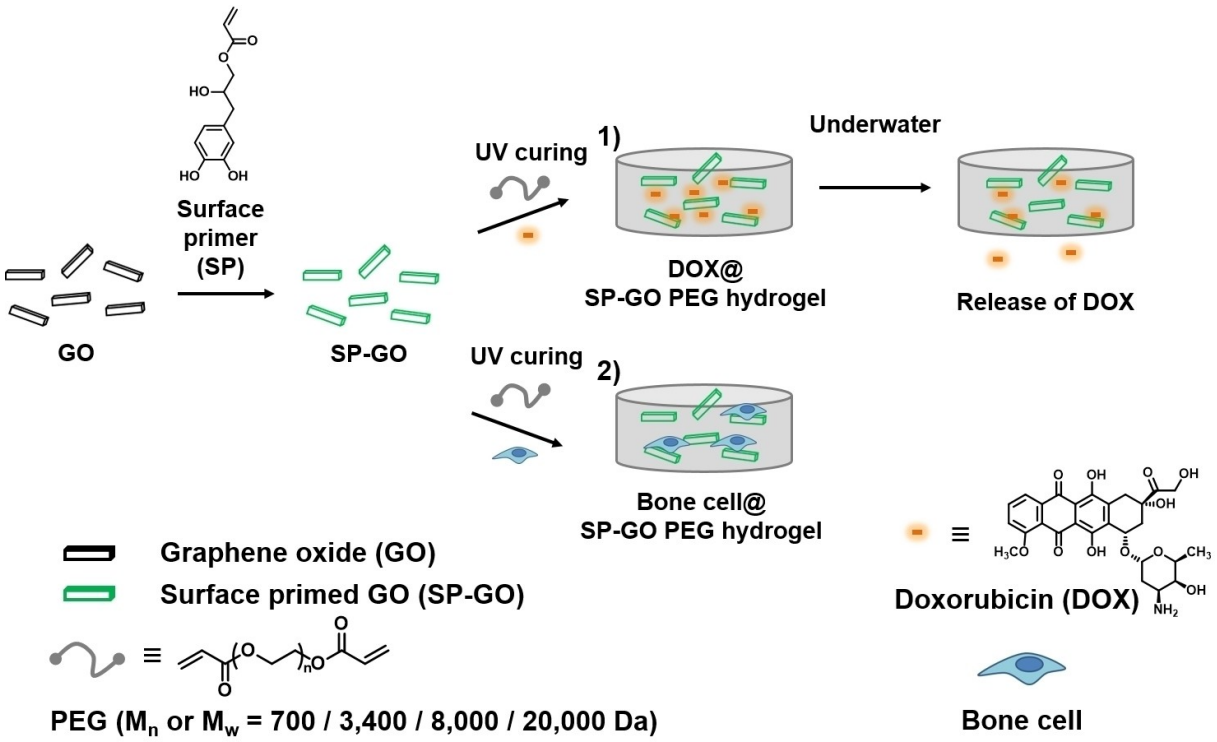

Figure 1. Schematic illustration of formulating PEG diacrylate hydrogel integrated with acrylated graphene oxide using acrylic surface primers. Two experimental studies using the acrylated graphene oxide-embedded hydrogels, how the graphene oxide effect on: 1) underwater release of the embedded aromatic drug, e.g., doxorubicin from the hydrogel, and 2) cell growth and adhesion used for a hydrogel-based tissue scaffold.

© 2020 Wiley-VCH Verlag GmbH & Co. KGaA, Weinheim

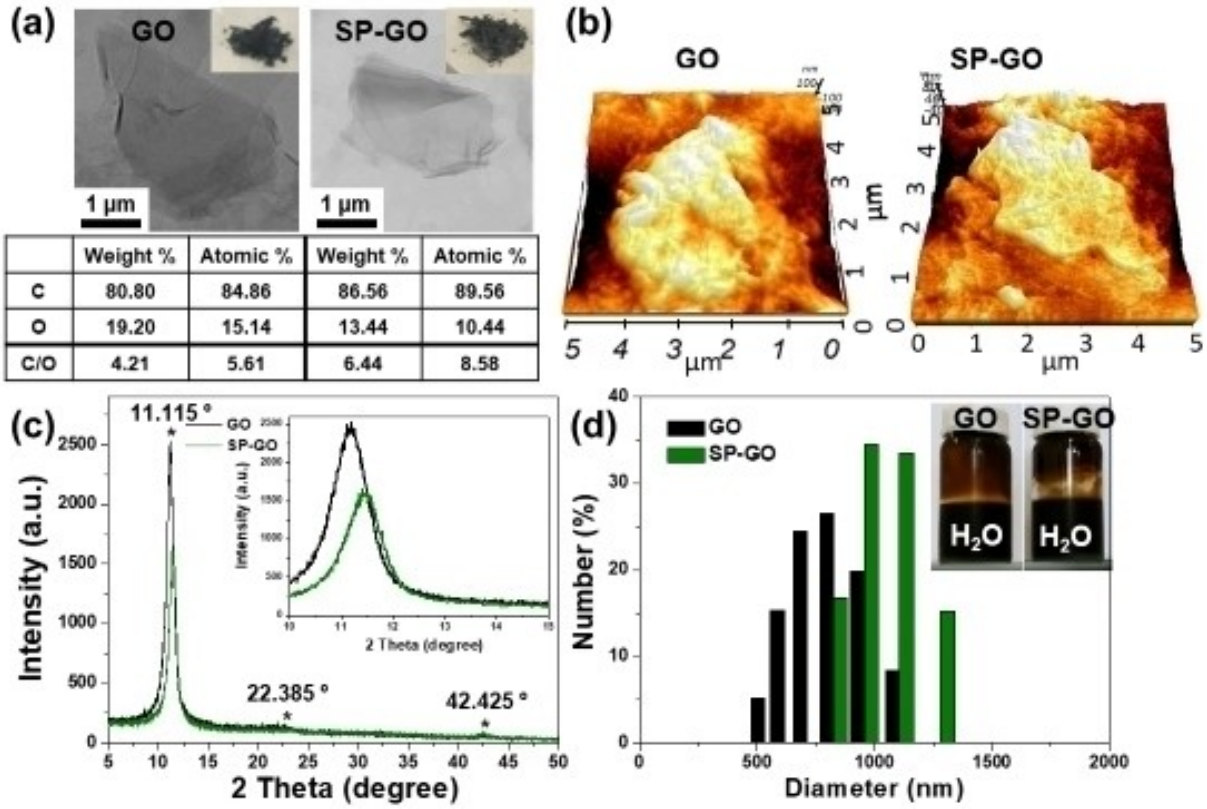

	Weight %	Atomic %	Weight %	Atomic %
C	80.80	84.86	86.56	89.56
O	19.20	15.14	13.44	10.44
C/O	4.21	5.61	6.44	8.58

Figure 2. (a) TEM images and EDS analysis of GO and SP-GO, inset: photograph of GO and SP-GO powder. (b) AFM images of GO and SP-GO. (c) XRD spectra of GO and SP-GO. (d) Size distribution of GO and SP-GO in the aqueous, inset: photograph of GO and SP-GO suspension in DI water.

property of GO and SP-GO. The sharp diffraction peak at $2\theta = 11.115^{\circ}$ corresponds to the (001) plane of GO, with a *d*-spacing of 0.79 nm, which is similar to the value obtained in previous studies.[4,5,38] The intensity of the diffraction peak of SP-GO was reduced compared with that of GO, which is caused by the formation of a surface priming layer between the GO sheets. After complete thermal decomposition of SP-GO, TGA curve exhibits that 18.2 wt% of GO is existent in SP-GO (**Figure S2**).

In general, hydrophilic GOs were dispersed in DI water (inset in Figure 2d). After surface primer treatment, hydrophobic SP-GO was dispersed in DI water as well. The zeta potential of GO and SP-GO dispersion in DI water was −36.1 mV and −32.4 mV, respectively, with a size distribution of 0.5–1.5 μm in diameter (Figure 2d). The lower zeta potential for the SP-GO dispersion is attributed to the adsorption of the nonpolar surface primer on the surface of GO. Moreover, the dispersion ability of SP-GO in a polar solvent, e.g., water or methanol, was reduced compared to that of GO due to surface adsorption (or priming) of the hydrophobic surface primer (**Figure S3**).

The acrylates of SP-GO were crosslinked with PEG diacrylate (PEG, $M_n = 700$ / $M_w = 8{,}000$ / $M_n = 20{,}000$ Da) during 10 min of 254 nm UV irradiation, yielding an SP-GO PEG hydrogel. The swelling ratio of SP-GO PEG hydrogel was compared with that of PEG hydrogel (Figure 3a) to investigate the effect of SP-GO on the properties of the PEG-based hydrogel.

After 1 hour immersion of the prepared hydrogels in DI water, no noticeable difference in the swelling ratio of the PEG hydrogel was found without or with SP-GO. This indicates that SP-GO did not disrupt the swelling property of the PEG hydrogels. Among the three different molecular weight-based PEG hydrogels tested, PEG hydrogels with molecular weight ($M_w = 8{,}000$ Da) showed the highest swelling ratio ($Q_s = 15 \sim 20$). The PEG hydrogels having M_n of 20,000 Da did not produce firm hydrogels during the 10 min of UV curing, demonstrating an irreproducible formulation and swelling ratio. Hence, two molecular weight-based hydrogels will be focused on in further studies ($M_n = 700$ and $M_w = 8{,}000$ Da).

The inner structures of the swollen SP-GO PEG hydrogels and PEG hydrogels were observed through SEM images (Figure 3b). While the hydrogels with $M_w = 8{,}000$ Da presented evident 10–20 μm-sized porous structures, the hydrogels with $M_n = 700$ Da were fewer in number and had a smaller pore size on the surface. These architectures certainly contributed to the different swelling ratios, as shown in Figure 3a.

The mechanical behavior of hydrogels with and without SP-GO was evaluated through compression tests to investigate the effect of SP-GO on the mechanical properties of PEG-based hydrogels. A representative stress-strain curve for each of the three hydrogel samples is described in Figure 4a.

All tested stress-strain curves are shown in **Figure S4**. Overall, the elastic modulus, ultimate strength, and toughness

© 2020 Wiley-VCH Verlag GmbH & Co. KGaA, Weinheim

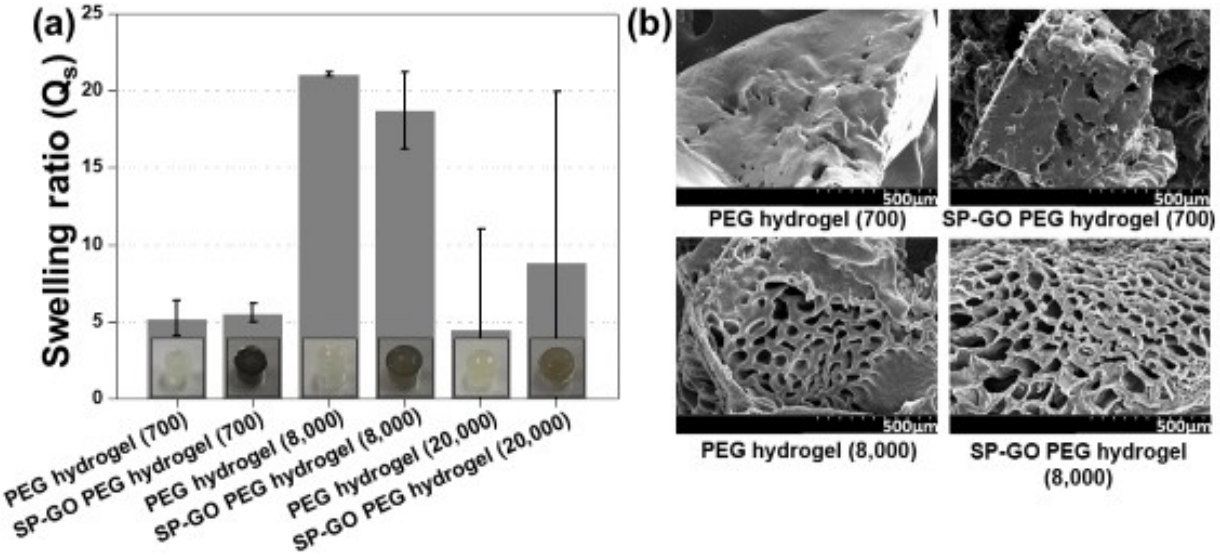

Figure 3. (a) Swelling ratio of PEG (M_n = 700 / M_w = 8,000 / M_n = 20,000 Da) hydrogels and SP-GO PEG hydrogels, inset: photograph of the hydrogels. (b) SEM images of the PEG (M_n = 700 / M_w = 8,000 Da) hydrogels and SP-GO PEG hydrogels.

of the hydrogels with M_w = 8,000 Da were higher than the hydrogels with M_n = 700 Da. The mechanical values of the SP-GO PEG hydrogels are comparable with those of PEG hydrogels within the same molecular weight range. Thus, SP-GO did not significantly change the basic mechanical and material properties of hydrogels due to a small amount of SP-GO (0.0045 wt%) entrapped in the hydrogels.

Time-dependent release profiles of aromatic DOX were conducted to explore how SP-GO influences the release of aromatic compounds from hydrogels. DOX, as a model anticancer drug, was co-mixed with a mixture of SP-GO/PEG in aqueous solution right before UV curing. Since the surface of GO is known to interact with the aromatic DOX by π-π stacking and hydrophobic interactions,[1,23,24] we assumed that SP-GO could trap DOX within the composite hydrogels, creating different kinds of sustained release profiles.

In Figure 5a, the entrapment efficiency of DOX in the PEG hydrogel and SP-GO PEG hydrogel (M_n = 700 Da) was 83.75% and 81.75%, respectively. The entrapment efficiency of DOX in the PEG hydrogel and SP-GO PEG hydrogel (M_w = 8,000 Da) was 99.90% and 90.15%, respectively. We supposed that the high loading efficiency of DOX in the PEG-based hydrogels resulted from a UV curing method that minimized the loss of inserted DOX.

The DOX from SP-GO PEG hydrogels was released in a sustained manner, and this amount compared with that of PEG hydrogels within the same molecular weight range (Figure 5b). At 120 hours (5 days) of underwater immersion, SP-GO hydrogels released 70.56% of the initially inserted DOX from the PEG hydrogel with M_w = 8,000 Da and 35.98% of the initially inserted DOX from PEG hydrogel with M_n = 700 Da in a sustained manner. These release amounts were slower or lesser than the released DOX from the PEG hydrogel (92.29% of the initially inserted DOX from PEG hydrogel with M_w = 8,000 Da, and 56.79% of the initially inserted DOX from PEG hydrogel with M_n = 700 Da). We believe that the reduced release profile of the hydrogels with SP-GO depends on various interactions such as constrained release from the hydrogel networks, π-π stacking,[1,23] hydrophobic interactions,[24] and electrostatic interactions between the aromatic DOX and SP-GO. The negatively charged SP-GO (-32.4 mV) attracted the positively charged DOX, partially contributing to the sustained release of DOX as well.

To check whether the measured release profile matches the theoretical release, the release of DOX was described by the exponential decay mass transfer model[39,40], which is given by Eq. (1),

$$\frac{M_t}{M_i}(\%) = \left(1 - e^{-(K\alpha).t}\right) \times 100 \quad (1)$$

Where M_i and M_t are the mass of DOX initially present in the hydrogel and released by the time t, respectively. $K\alpha$ (hour^{-1}) is the volumetric mass transfer coefficient. The values of $K\alpha$ can be determined by fitting the experimental data with the predictions of equation (1) (Figure 5b). The model could describe the experimental data well in indicating that the release of DOX from the hydrogel is dominantly driven by diffusive mass transfer with preserving stable hydrogel network. Table 1 lists the values of $K\alpha$ for various hydrogels. A release of DOX is apparent in the first 24 hours for the PEG-based hydrogels. This result can be attributed to a higher DOX concentration gradient between the hydrogel and the surrounding environment at the beginning of release experiments.[41] This conclusion implies indirectly that the reduced release profile of DOX from the SP-GO PEG hydrogel is from the attraction of DOX toward SP-GO, compared with that from the PEG hydrogel.

© 2020 Wiley-VCH Verlag GmbH & Co. KGaA, Weinheim

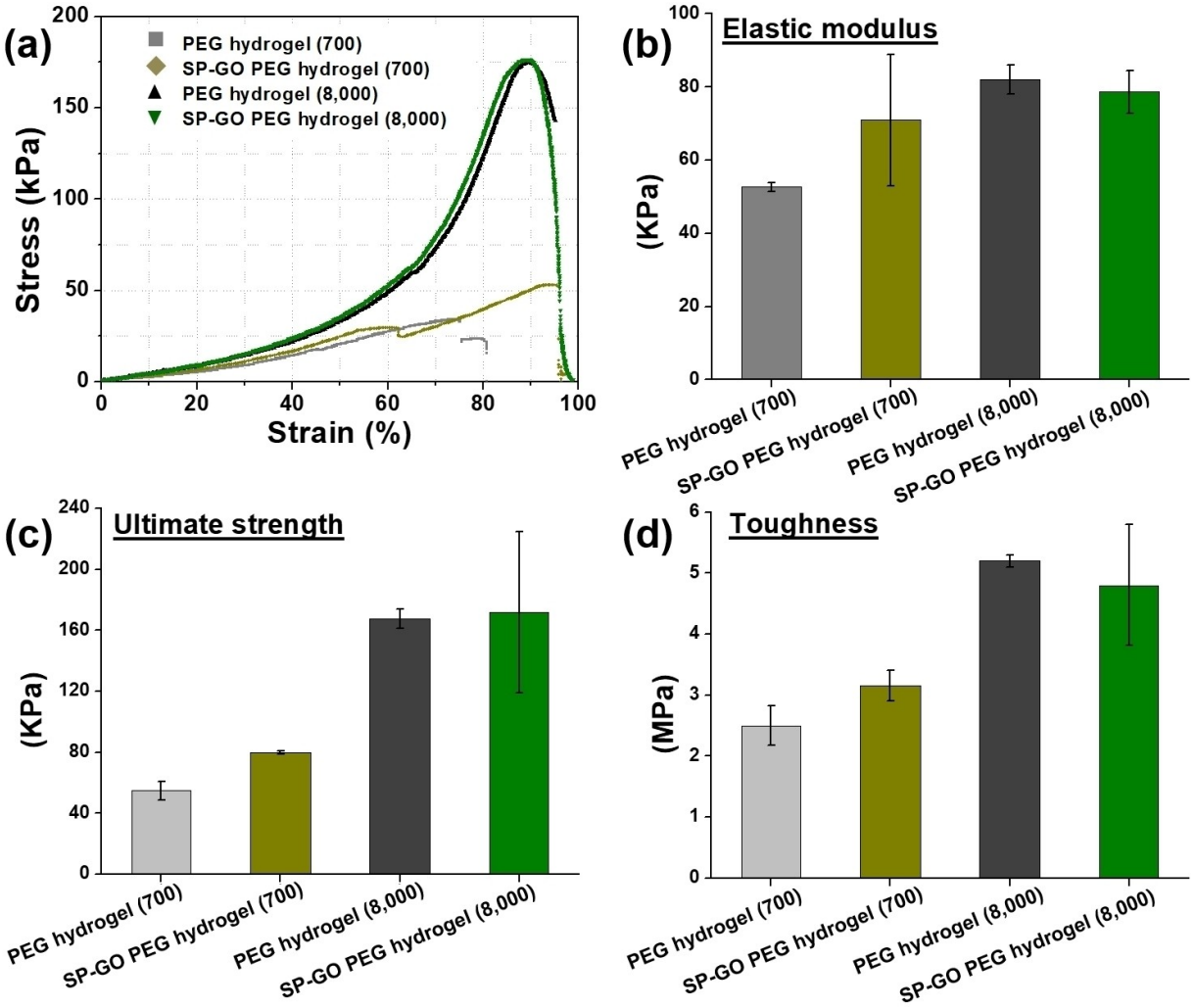

Figure 4. (a) Representative stress-strain curve of PEG ($M_n = 700$ / $M_w = 8{,}000$ Da) hydrogels and SP-GO PEG hydrogels. (b-d) Elastic modulus, ultimate strength, and toughness of the hydrogels.

Table 1. The values of the volumetric mass transfer coefficient ($K\alpha$) for various hydrogels obtained by fitting the model to the experimental data.

Hydrogels	$K\alpha$ (hour^{-1})
PEG hydrogel (8,000)	0.021
SP-GO PEG hydrogel (8,000)	0.013
PEG hydrogel (700)	0.008
SP-GO PEG hydrogel (700)	0.004

Bone MG-63 cells were entrapped in PEG-based hydrogels with a molecular weight of $M_w = 3{,}400$ Da for demonstrating the potential of the SP-GO hydrogel as a tissue scaffold, which could be a way to reduce toxicity in cell viability tests[35,42,43] and porous structures,[42] which is similar to our observation in the SEM images for the PEG-basedse hydrogels ($M_w = 8{,}000$ Da).

In Figure 6a and **6 b**, comparable numbers and morphology of MG-63 cells were shown in both the PEG hydrogel and the SP-GO PEG hydrogel observed by optical microscopic images from the bottom side of the hydrogels. SP-GO PEG hydrogels entrapped with MG-63 cells (MG-63 cell@SP-GO PEG hydrogels) showed a brownish color due to the presence of SP-GO. To investigate the inner structures of the hydrogels, SEM images of hydrogel cross-sections were recorded (Figure 6c and **6 d**). No significant difference in numbers and cell morphology between MG-63 cell@PEG hydrogel and MG-63 cell@SP-GO PEG hydrogel was detected in the aspect of the microscopic scale. In Figure 6e, an enzyme-linked immunosorbent assay (ELISA) was conducted in which cell culture times were varied from 0–10 days to compare the TGF-β expression level (closely related to osteoblasts[44,45]) from the hydrogels. A slightly increased amount of TGF-β from the MG-63 cell@SP-GO PEG hydrogel was measured compared with that from the MG-63 cell@PEG hydrogel. Moreover, the Western blot immunoassay of the hydrogels was conducted to observe the expression level of fibronectin, which is associated with cell adhesion and growth.[46,47] In Figure 6f, an increased band intensity appeared for the MG-63 cell@SP-GO PEG hydrogel compared with that for the MG-63 cell@PEG hydrogel. From the results of ELISA and the Western blot, it can be concluded that SP-GO enhanced

© 2020 Wiley-VCH Verlag GmbH & Co. KGaA, Weinheim

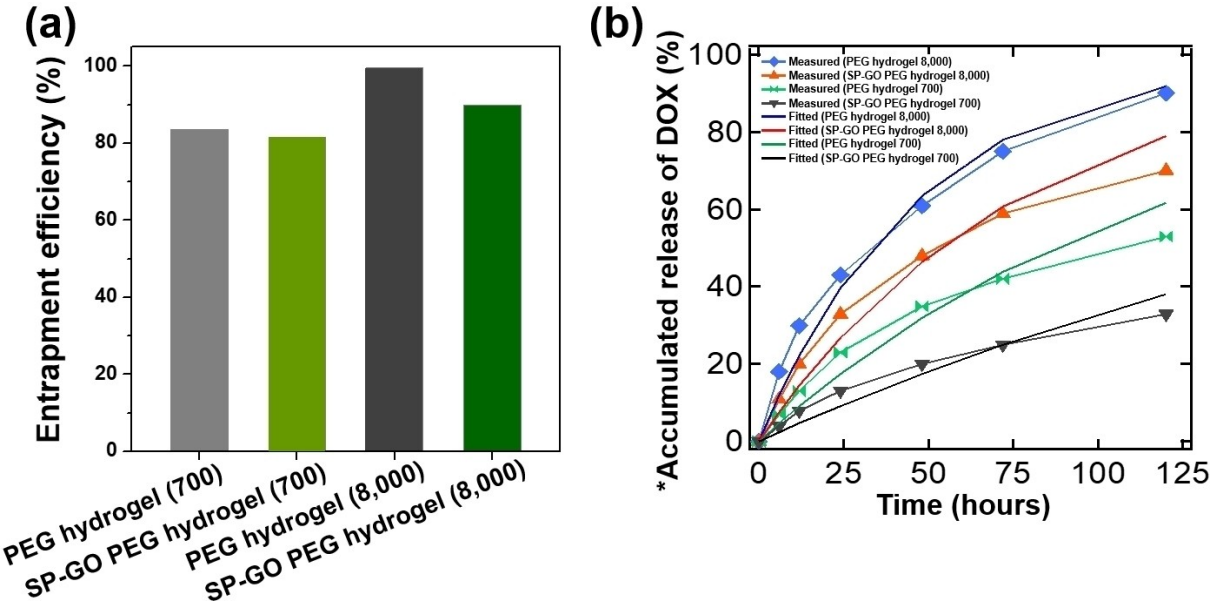

Figure 5. (a) Entrapment efficiency of DOX in PEG ($M_n = 700$ / $M_w = 8{,}000$ Da) hydrogels and SP-GO PEG hydrogels. (b) Plot of measured and fitted accumulated release of DOX for the hydrogels as a function of time under water. *The accumulated release of DOX is expressed as a percentage per the initial amount of entrapped DOX in the hydrogels.

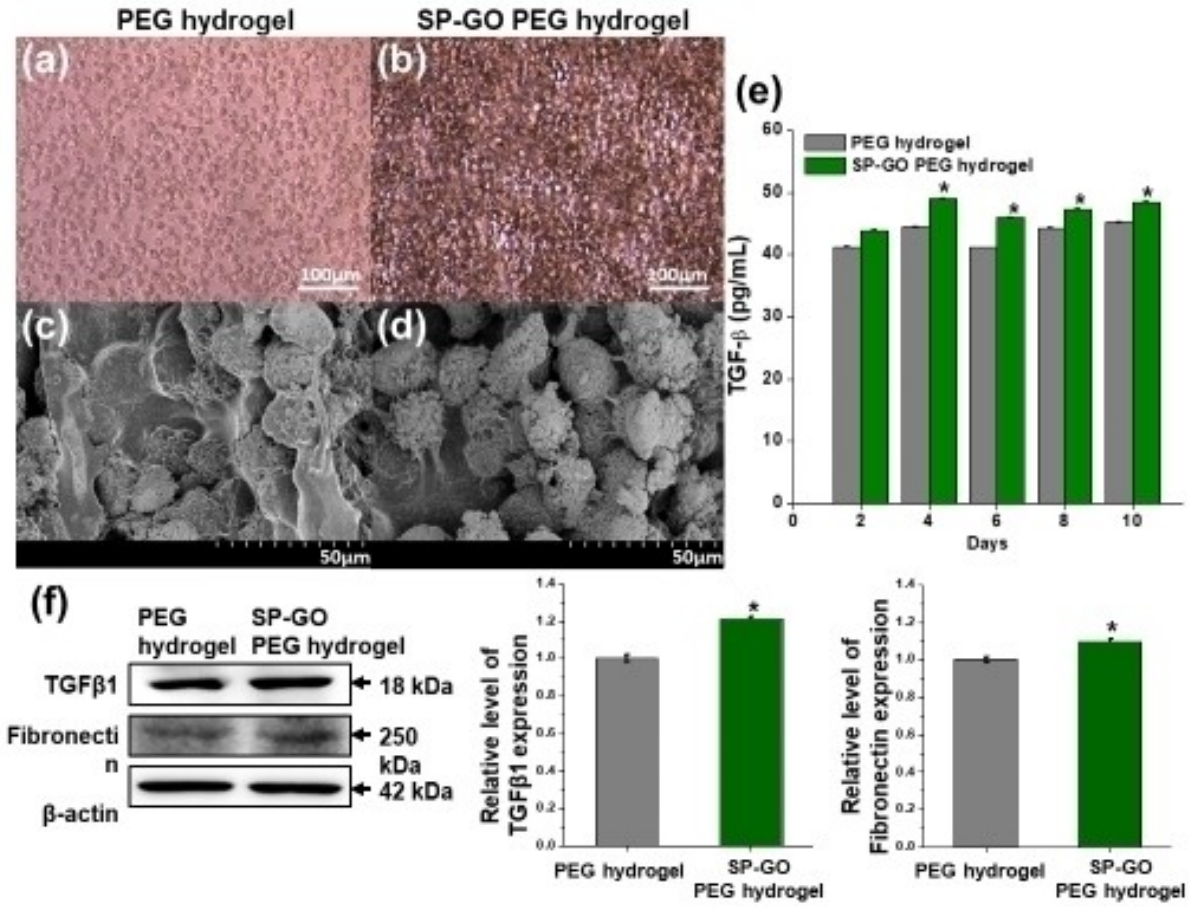

Figure 6. Optical microscopic images of MG-63 cell embedded hydrogels. (a) PEG hydrogel and (b) SP-GO PEG hydrogel after cultivation for 10 days. SEM images of cross-sectional region in (c) PEG hydrogel, (d) SP-GO PEG hydrogel. (e) Amount of TGF-β expressed from the hydrogels. (f) Images of Western blot from the hydrogels. *p*-values were calculated using the Tukey post hoc t-test to assess statistical certainty of the comparisons (*$p < 0.05$).

© 2020 Wiley-VCH Verlag GmbH & Co. KGaA, Weinheim

osteoblast cell growth and adhesion by providing a cell-laid scaffold.[48]

Based on the two experimental studies of underwater release and cell-related protein expression levels, we can envision the sustained and slower release of aromatic drugs from the composite hydrogels and potential platforms of tissue scaffolds.

3. Conclusions

Without complex chemical reactions, acrylation of GO was modified using an acrylic surface primer, which had adhesive phenolics directed toward the GO and acrylate groups for photocrosslinking with acrylate-based materials. The inserted GO did not disrupt the mechanical behavior and materials property of PEG-based hydrogels. The composite hydrogels showed a sustained and slower anticancer drug, i.e., DOX release profiles compared with PEG hydrogels. Moreover, the acrylated GO enhanced expression levels of TGF-β and fibronectin which is associated with cell adhesion and growth in the osteoblast cell entrapped hydrogel scaffolds. From these results, we consider that reaction-free GO hydrogels could reduce the toxicity from chemical additives requiring chemical reactions and could be used as controlled-release drug delivery systems and tissue scaffolds.

Author Contributions

The manuscript was written through the contributions of all authors. All authors have approved the final version of the manuscript.

Notes

The authors declare no competing financial interest.

Supporting Information Summary

Information of materials in experiment, preparation and characterization methods of samples, Entrapment efficiency, DOX release kinetics, ELISA assay, and Western blot of PEG-based hydrogels are provided in the supporting information.

Acknowledgments

This work was supported by the National Research Foundation of Korea (NRF) grant funded by the Korea government (MSIP: Ministry of Science, ICT & Future Planning) (NRF-2018R1D1 A1B07050070). We thank Professor Jin-Woo Oh who kindly allowed us to use his AFM (Pusan National University).

Conflict of Interest

The authors declare no conflict of interest.

Keywords: acrylation · composite hydrogel · graphene oxide · surface primer · sustained release · tissue scaffolds

[1] T. P. Dasari Shareena, D. McShan, A. K. Dasmahapatra, P. B. Tchounwou, *Nano-Micro Lett.* **2018**, *10*, 53.
[2] D. R. Dreyer, R. S. Ruoff, C. W. Bielawski, *Angew. Chemie Int. Ed.* **2010**, *49*, 9336.
[3] S. Goenka, V. Sant, S. Sant, *J. Control. Release* **2014**, *173*, 75.
[4] P. Bhanja, S. K. Das, A. K. Patra, A. Bhaumik, *RSC Adv.* **2016**, *6*, 72055.
[5] S. Choudhary, H. P. Mungse, O. P. Khatri, *J. Mater. Chem.* **2012**, *22*, 21032.
[6] H. Lee, S. M. Dellatore, W. M. Miller, P. B. Messersmith, *Science (80-.).* **2007**, *318*, 426.
[7] T. S. Sileika, D. G. Barrett, R. Zhang, K. H. A. Lau, P. B. Messersmith, *Angew. Chemie Int. Ed.* **2013**, *52*, 10766.
[8] J. Ryu, S. H. Ku, H. Lee, C. B. Park, *Adv. Funct. Mater.* **2010**, *20*, 2132.
[9] S. H. Yang, S. M. Kang, K.-B. Lee, T. D. Chung, H. Lee, I. S. Choi, *J. Am. Chem. Soc.* **2011**, *133*, 2795.
[10] S. M. Kang, N. S. Hwang, J. Yeom, S. Y. Park, P. B. Messersmith, I. S. Choi, R. Langer, D. G. Anderson, H. Lee, *Adv. Funct. Mater.* **2012**, *22*, 2949.
[11] B. P. Lee, P. B. Messersmith, J. N. Israelachvili, J. H. Waite, *Annu. Rev. Mater. Res.* **2011**, *41*, 99.
[12] H. Lee, N. F. Scherer, P. B. Messersmith, *Proc. Natl. Acad. Sci.* **2006**, *103*, 12999.
[13] C. R. Matos-Pérez, J. D. White, J. J. Wilker, *J. Am. Chem. Soc.* **2012**, *134*, 9498.
[14] M. Mehdizadeh, H. Weng, D. Gyawali, L. Tang, J. Yang, *Biomaterials* **2012**, *33*, 7972.
[15] Y. Li, H. Meng, Y. Liu, A. Narkar, B. P. Lee, *ACS Appl. Mater. Interfaces* **2016**, *8*, 11980.
[16] M.-H. Ryou, J. Kim, I. Lee, S. Kim, Y. K. Jeong, S. Hong, J. H. Ryu, T.-S. Kim, J.-K. Park, H. Lee, J. W. Choi, *Adv. Mater.* **2013**, *25*, 1571.
[17] S. Das, B. H. Lee, R. T. H. Linstadt, K. Cunha, Y. Li, Y. Kaufman, Z. A. Levine, B. H. Lipshutz, R. D. Lins, J.-E. Shea, A. J. Heeger, B. K. Ahn, *Nano Lett.* **2016**, *16*, 6709.
[18] S. Seo, D. W. Lee, J. S. Ahn, K. Cunha, E. Filippidi, S. W. Ju, E. Shin, B.-S. Kim, Z. A. Levine, R. D. Lins, J. N. Israelachvili, J. H. Waite, M. T. Valentine, J. E. Shea, B. K. Ahn, *Adv. Mater.* **2017**, *29*, 1703026.
[19] X. Sun, Z. Liu, K. Welsher, J. T. Robinson, A. Goodwin, S. Zaric, H. Dai, *Nano Res.* **2008**, *1*, 203.
[20] K. Yang, L. Feng, H. Hong, W. Cai, Z. Liu, *Nat. Protoc.* **2013**, *8*, 2392.
[21] Y. Yang, A. M. Asiri, Z. Tang, D. Du, Y. Lin, *Mater. Today* **2013**, *16*, 365.
[22] X. Wu, S.-J. Ding, K. Lin, J. Su, *J. Mater. Chem. B* **2017**, *5*, 3084.
[23] L. Zhang, J. Xia, Q. Zhao, L. Liu, Z. Zhang, *Small* **2010**, *6*, 537.
[24] U. Dembereldorj, M. Kim, S. Kim, E.-O. Ganbold, S. Y. Lee, S.-W. Joo, *J. Mater. Chem.* **2012**, *22*, 23845.
[25] T. Zhou, X. Zhou, D. Xing, *Biomaterials* **2014**, *35*, 4185.
[26] S. Senapati, A. K. Mahanta, S. Kumar, P. Maiti, *Signal Transduct. Target. Ther.* **2018**, *3*, 7.
[27] X. Qi, W. Wei, J. Li, Y. Liu, X. Hu, J. Zhang, L. Bi, W. Dong, *ACS Biomater. Sci. Eng.* **2015**, *1*, 1287.
[28] S. Singh, A. Mishra, R. Kumari, K. K. Sinha, M. K. Singh, P. Das, *Carbon N. Y.* **2017**, *114*, 169.
[29] S. Jin, J. Wan, L. Meng, X. Huang, J. Guo, L. Liu, C. Wang, *ACS Appl. Mater. Interfaces* **2015**, *7*, 19843.
[30] M. Singh, S. Kundu, A. Reddy M, V. Sreekanth, R. K. Motiani, S. Sengupta, A. Srivastava, A. Bajaj, *Nanoscale* **2014**, *6*, 12849.
[31] Q. Xue, H. Ren, C. Xu, G. Wang, C. Ren, J. Hao, D. Ding, *Sci. Rep.* **2015**, *5*, 8764.
[32] C. G. Williams, T. K. Kim, A. Taboas, A. Malik, P. Manson, J. Elisseeff, *Tissue Eng.* **2003**, *9*, 679.
[33] T. Jiang, J. Zhao, S. Yu, Z. Mao, C. Gao, Y. Zhu, C. Mao, L. Zheng, *Biomaterials* **2019**, *188*, 130.
[34] S. J. Bryant, K. S. Anseth, *Biomaterials* **2001**, *22*, 619.
[35] M. Noh, S.-H. Kim, J. Kim, J.-R. Lee, G.-J. Jeong, J.-K. Yoon, S. Kang, S. H. Bhang, H. H. Yoon, J.-C. Lee, N. S. Hwang, B.-S. Kim, *RSC Adv.* **2017**, *7*, 20779.
[36] S. Kang, J. B. Park, T.-J. Lee, S. Ryu, S. H. Bhang, W.-G. La, M.-K. Noh, B. H. Hong, B.-S. Kim, *Carbon N. Y.* **2015**, *83*, 162.
[37] Y. Luo, H. Shen, Y. Fang, Y. Cao, J. Huang, M. Zhang, J. Dai, X. Shi, Z. Zhang, *ACS Appl. Mater. Interfaces* **2015**, *7*, 6331.

© 2020 Wiley-VCH Verlag GmbH & Co. KGaA, Weinheim

[38] W. Gao, Y. Lu, Y. Chao, Y. Ma, B. Zhu, J. Jia, A. Huang, K. Xie, J. Li, Y. Bai, *J. Phys. Chem. C* **2017**, *121*, 21685.
[39] J. Crank, *The Mathematics of Diffusion*, Oxford University Press, New York, **1979**.
[40] C. X. (Cynthia) Lin, S. Z. Qiao, C. Z. Yu, S. Ismadji, G. Q. (Max) Lu, *Microporous Mesoporous Mater.* **2009**, *117*, 213.
[41] A. Nieto, M. Colilla, F. Balas, M. Vallet-Regí, *Langmuir* **2010**, *26*, 5038.
[42] K. Son, J. Lee, *Materials (Basel).* **2016**, *9*, 854.
[43] V. Chan, P. Zorlutuna, J. H. Jeong, H. Kong, R. Bashir, *Lab Chip* **2010**, *10*, 2062.
[44] F. Massicotte, D. Lajeunesse, M. Benderdour, J.-P. Pelletier, G. Hilal, N. Duval, J. Martel-Pelletier, *Osteoarthr. Cartil.* **2002**, *10*, 491.
[45] B. Hopwood, A. Tsykin, D. M. Findlay, N. L. Fazzalari, *Arthritis Res. Ther.* **2007**, *9*, R100.
[46] J.-Y. Kim, J.-Y. Choi, J.-H. Jeong, E.-S. Jang, A.-S. Kim, S.-G. Kim, H.-Y. Kwon, Y.-Y. Jo, J.-H. Yeo, *BMB Rep.* **2010**, *43*, 52.
[47] R. Pankov, *J. Cell Sci.* **2002**, *115*, 3861.
[48] F. M. Watt, W. T. S. Huck, *Nat. Rev. Mol. Cell Biol.* **2013**, *14*, 467.

Submitted: January 15, 2020
Accepted: May 6, 2020

© 2020 Wiley-VCH Verlag GmbH & Co. KGaA, Weinheim